Proceedings

Fuzzy Logic Modeling for Integrating the Thematic Layers Derived from Remote Sensing imagery: A Mineral Exploration Technique †

Abstract: In this study, fuzzy logic modeling was implemented to fuse the thematic layers derived from Principal Component analysis (PCA) technique for generating mineral prospectivity maps. Advanced Spaceborne Thermal Emission and Reflection Radiometer (ASTER) and WorldView-3 satellite remote sensing data were used. A spatial subset zone of the Central Iranian Terrane (CIT), Iran was selected in this study. The PCA techniques was implemented for the processing of the datasets and producing alteration thematic layers. The PCA4, PCA5 and PCA8 were selected as the most rational alteration thematic layers of ASTER for generating prospectivity map. The fuzzy gamma operator was used to fuse the selected alteration thematic layers. The PCA3, PCA4 and PCA6 thematic layers (most rational alteration thematic layers) of WV-3 were fused using fuzzy AND operator. Field reconnaissance, X-ray diffraction (XRD) analysis and Analytical spectral devices (ASD) spectroscopy were carried out to verify the image processing results. Subsequently, mineral prospectivity maps were produced showing high potential zones of Pb-Zn mineralization in the study area.

Keywords: ASTER; WorldView-3; fuzzy logic modeling; mineral exploration

1. Introduction

Remote sensing satellite imagery has been applied to detect alteration minerals, specifically dolomite and gossan zone (Govil et al., 2018; Pour et al., 2018a,b,c,2019a,b,c). A variety of image processing techniques were previously used to map of hydrothermal alteration minerals. However, fusing the most rational thematic layers to generate a comprehensive mineral prospectivity map for sediment-hosted Pb-Zn exploration was neglected. Fuzzy logic modeling has been successfully used for mineral prospectivity mapping in metallogenic provinces. Fuzzy logic modeling for mineral prospectivity mapping typically incorporates three main stages, including fuzzification of evidential data, logical combination of fuzzy evidential maps with the support of an inference network and proper fuzzy set operations and defuzzification of fuzzy mineral prospectivity output in order to aid its interpretation (Kim et al., 2019). The CIT area (Figure 1) contains great potential for carbonate-hosted Pb-Zn deposits (Rajabi et al., 2012). There is no comprehensive study to map hydrothermal alteration mineral zones in this area, yet. In this research, ASTER and WorldView-3 (WV-3) satellite remote sensing data were used for prospectivity mapping. The main objective of this analysis is implementing PCA technique to ASTER and WV-3 to generate mineral prospectivity maps using fuzzy logic modeling.

2. Geologic setting of the study area

Three fault systems are documented in the CIT area, including Nayband and Nehbandan faults, Poshteh-Badam and Kalmard faults and Kuhbanan and Rafsanjan faults. The occurrence of magmatism in the area is associated with a back-arc extension zone (Samani, 1988). The sediment-hosted Pb-Zn mineralization in the study area is formed during synchronous faulting activities with sedimentation, detrital sedimentation associated with faulting activities, replacement of rhyolitic volcanic rocks and formation of rift sediments and subsidence (Samani, 1988).

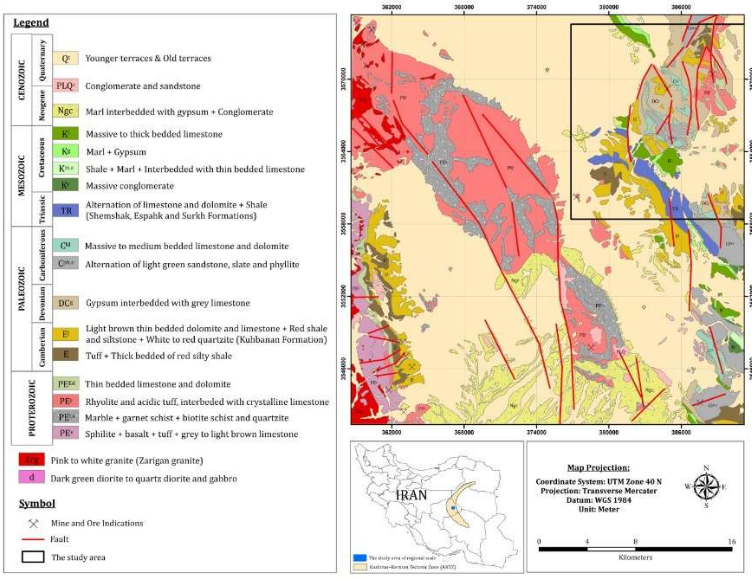

Figure 1. Geology map of the study area (modified from Chadormalo geology map, 1:100000, sheet No:71, Geological Survey and Mineral Exploration of Iran (GSMEI)). Black cube delimits ASTER imagery.

3. Materials and methods

3.1. Data characteristics

ASTER and WV-3 was utilized in this analysis. ASTER has three bands in visible and near infrared (VNIR) (0.52 and 0.86 μm), six bands in shortwave infrared (SWIR) (1.6 to 2.43 μm) and five bands in thermal infrared (TIR) (8.125 to 11.65 μm) with 15 m,30 m and 90 m spatial resolutions, respectively (Abrams et al., 2015). ASTER strip size is 60km. WV-3 has eight spectral bands in the VNIR wavelength region (1.24 m spatial resolution) and for eight spectral bands in the SWIR (3.7 m spatial resolution) with strip size of 13 km (Kuester, 2016). An ASTER scene cloud-free level 1T product and A level 2 A WV-3 data covering the study area were processed in this study.

3.2. Image processing

3.2.1. Principal Components Analysis (PCA)

The PCA is a mathematical technique that transforms a quantity of correlated variables into a number of uncorrelated linear variables called PCs (Gupta et al., 2013). In this analysis, the PCA method was implemented based on covariance matrix to ASTER (VNIR+SWIR bands) and WV-3 (VNIR bands) for identifying hydrothermal alteration mineral assemblages in the study area. Table 1 (A-B) shows eigenvector matrix for the selected bands of the remote sensing datasets.

3.2.2 Fuzzy logic modeling

Fuzzy logic modeling was proposed by Zadeh (1965). It is a form of many-valued logic in which the truth values of variables may be any real number between 0 and 1 both inclusive (Novák et al., 1999). A fuzzy set of A is a set of ordered pairs:

$$A = \{(x, \mu_A(x)) \mid x \in X\} \quad (1)$$

where μ_A (x) is termed the membership function or membership grade of x in A. μ_A (x) maps x to membership space (M), when M contains only the two points 0 and 1. The range of μ_A (x) is [0, 1], where zero expresses non-membership and one expresses full membership (Zadeh 1965). A set of fuzzy membership values is stated in a continuous series from 0 to 1.

Table 1. Eigenvector matrix derived from PCA for the selected bands of the remote sensing datasets used in this study. (A) ASTER bands (VNIR+SWIR); (B) WV3 band (1 to 8 VNIR).

(C)Eigenvector	Band 1	Band 2	Band 3	Band 4	Band 5	Band 6	Band 7	Band 8	Band 9
PCA 1	0.306376	0.354156	0.357999	0.373947	0.327957	0.351186	0.312760	0.294817	0.311584
PCA 2	-0.506185	-0.503027	-0.377710	0.175856	0.271555	0.270302	0.240492	0.247816	0.226041
PCA 3	-0.277958	-0.020633	0.232513	0.555288	0.118013	0.231883	-0.218093	-0.635404	-0.202253
PCA 4	-0.123343	-0.657125	-0.626671	0.626671	0.219378	0.135436	-0.037673	-0.233067	-0.106928
PCA 5	-0.005336	-0.013068	-0.049688	0.544534	-0.082811	-0.437342	0.180406	0.400661	-0.556429
PCA 6	0.269821	-0.516554	0.233199	0.285564	-0.309355	-0.365753	0.067872	-0.145724	0.518769
PCA 7	-0.209453	0.529334	-0.464617	0.294560	-0.485018	-0.017691	-0.005474	-0.049871	0.367733
PCA 8	0.027679	-0.039707	0.000725	0.469109	0.336338	-0.003040	-0.870266	0.409042	0.160571
PCA 9	0.152864	-0.239013	0.098348	0.029191	-0.632661	0.637281	-0.028538	0.205046	-0.244409

(D)Eigenvector	Band 1	Band 2	Band 3	Band 4	Band 5	Band 6	Band 7	Band 8
PCA 1	-0.314986	-0.330951	-0.348156	-0.359256	-0.364601	-0.367182	-0.369097	-0.370119
PCA 2	0.655926	0.454510	0.183457	-0.046042	-0.154854	-0.251952	-0.320189	-0.370709
PCA 3	-0.331273	-0.598506	0.354295	-0.129646	0.661001	-0.220796	0.341420	0.108973
PCA 4	-0.244961	0.345377	0.145561	0.631659	0.012267	0.368220	-0.509311	-0.142316
PCA 5	-0.384633	0.279151	0.433976	-0.092808	0.081588	-0.370014	-0.142544	0.187618
PCA 6	0.236442	-0.427799	-0.515988	-0.065670	0.646312	0.248715	0.043257	0.095274
PCA 7	0.257771	-0.301701	-0.070317	-0.389055	0.471694	0.225588	-0.427691	0.035215
PCA 8	0.174655	-0.560947	0.307690	-0.163685	-0.332755	0.108819	0.068151	-0.001993

3.3.5. Fieldwork Data and Laboratory Analysis

GPS survey, X-ray diffraction (XRD) analysis and Analytical spectral devices (ASD) spectroscopy were carried out in the study area and preformed to the samples collected from the main lithological units exposed, respectively.

4. Results and discussion

The PCA technique was also implemented on the spatial selected subset of ASTER for mapping alteration minerals. The eigenvector matrix for ASTER VNIR+SWIR bands is shown in Table 1 (A). The PC3 has 0.555288 loading in band 4 and -0.635404 loading in band 8. The chlorites and carbonate show high reflectance about 1.6 μm (band 4 of ASTER), while absorption features at 2.350 μm, (bands 8 of ASTER) (Mars and Rowan, 2010,2011). Therefore, the PC3 is considered as a thematic layer. The PC4 has -0.657125 loadings in band 2 and 0.626671 loadings in band 4 (Table 1 A). Iron oxide/hydroxides minerals illustrate by strong absorption at 0.40 to 1.10 μm and reflection about 1.60 μm (Hunt and Ashley, 1979). Seeing the spectral location of bands 2 and 4 of ASTER, it is discernable that the PC4 image as a thematic layer. The PC5 shows 0.544534 loading in band 4 and -0.437342 loading in band 6 and -0.556429 loading band 9 (Table 1 A). The sulfate minerals display absorption features at 2.20 to 2.50 μm (Clark, 1999), corresponding to bands 6 to 9 of ASTER. Consequently, sulfate minerals can be mapped in the PC5 image as a thematic layer. Carbonate minerals have diagnostic CO3 spectral absorptions near 2.35 μm, which can be significantly used to identify carbonate-bearing rocks (Clark 1999). The carbonate minerals such as calcite and dolomite show distinctive narrow absorption features around 2.35 μm analogous to band 8 (2.295–2.365 μm) of ASTER data (Mars and Rowan, 2010). Thus, PC8 image has information related to the spatial distribution of dolomite. The PC8 has 0.469109 loading in band 4 and 0.336338 loading band 5, in addition 0.870266 loading in band 7 (Table 1 A). The PC8 image was also considered as a thematic layer.

The PCA statistical results for the WV-3 bands shows the PC3, PC4 and PC6 can be considered as thematic layers for mapping iron-stained alteration, dolomite/Fe^{2+} and Fe^{3+}oxides, respectively. The PC3 has -0.598506 loading in band 2 and 0.661001 loading in band 5 (Table 1 B) for mapping iron-stained alteration. The PC4 shows 0.345377 loading in band 2 and 0.631659 loading in band 4 as well as -0.509311 loading in band 7 (Table 1 B) for identification of dolomite/Fe^{2+}. The PC6 contains -0.427799 in band 2 and (-0.515988 loading band 3, while 0.646312 loading in band 5 (Table 1 B) for mapping Fe^{3+}oxides.

Mineral prospectivity maps were produced of alteration thematic layers using fuzzy-logic model (Table 3). The alteration thematic layers of ASTER were integrated using the fuzzy gamma operator (γ=0.6) (Table 3). ASTER prospectivity map shows the high value (0.7 to 1.0) of the favorability index as prospective zones (Figure 2). However, the highest value (0.9 to 1.0) of the favorability index can be considered the high prospective zones for Pb-Zn mineralizations, which overlap to documented Pb-Zn occurrences alongside fault systems (Figure 2).

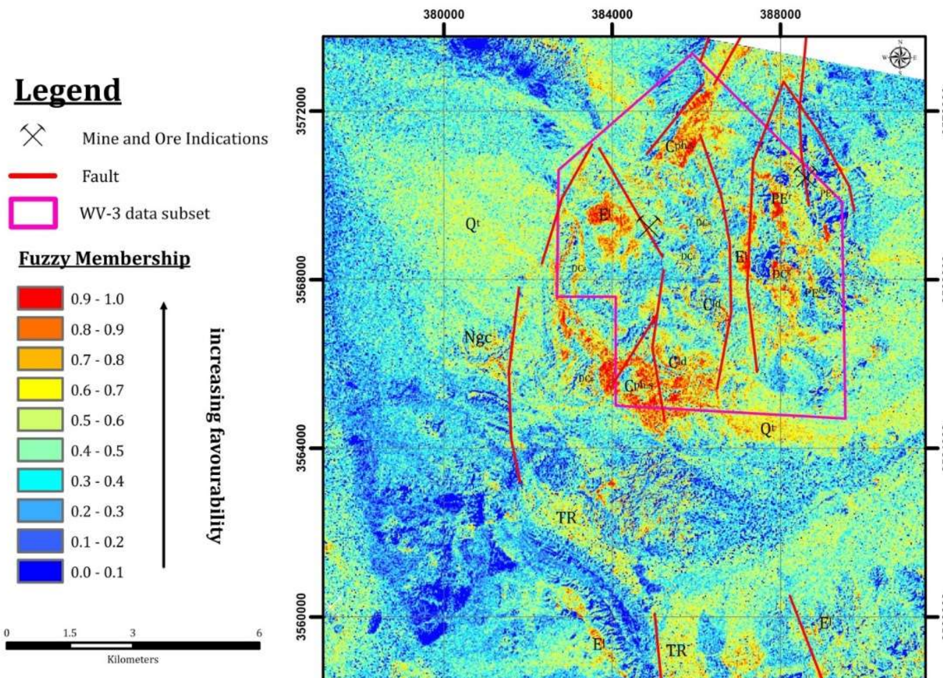

Figure 2. Mineral prospectivity map derived from ASTER selected alteration thematic layers.

Figure 3 shows prospectivity map derived from alteration thematic layers of WV-3 data. The fuzzy AND operator was implemented to fuse the selected alteration thematic layers (Table 3). The highest value of (0.8 to 1.0) the favorability index is obtained for few parts and a high value (0.6 to 0.9) of the favorability index in some parts of the study area. The Pb-Zn mineralization zones contain high favorability index value (0.6 to 1.0) and are also connecting to fault systems at the local scale (Figure 3). Accordingly, the most favorable/prospective zones for Pb-Zn mineralization in the study area are in fault contact zones with impermeable lithological units.

Table 3. Fuzzification parameters for the thematic layers.

Data Origin	Input Layer	Detection	Membership Type	Fuzzy Operator
ASTER Dataset	PC4	Iron oxide/hydroxides minerals	Linear	Gamma (γ=0.6)
	PC5	OH/S-O/CO3-bearing minerals		
	PC8	Dolomite		
World-View3 Dataset	PC3	All iron oxides	Linear	AND
	PC4	Dolomite/Fe^{2+} oxides		
	PC6	Fe^{3+} oxides		

The argillic alteration, sericitic zones, iron oxides and dolomitization were found in during fieldwork. Several surface expressions of hematite, malachite, pyrite, galena and sphalerite were observed. Surface expression of Pb-Zn mineralization was typically detected in the fault contact of dolomite with other lithological units in several parts of the study area. The XRD analysis reveals the presence of quartz, dolomite, calcite, muscovite, chlorite, gypsum, albite, illite, jarosite and malachite. The ASD analysis for shale, gypsum, dolomite and calcite was measured, which shows some typical absorption features about 1.40 μm attributed to OH/H2O stretches, 1.90 μm related to H2O stretches, 2.20 μm due to combination of the OH-stretching fundamental with Al-OH bending mode (Al-rich phyllosilicates), the absorption feature near 2.20 μm is related to S-O bending mode and absorption features related to Fe^{2+} at 0.9 to 1.2 μm and CO_3 in 2.35 μm.

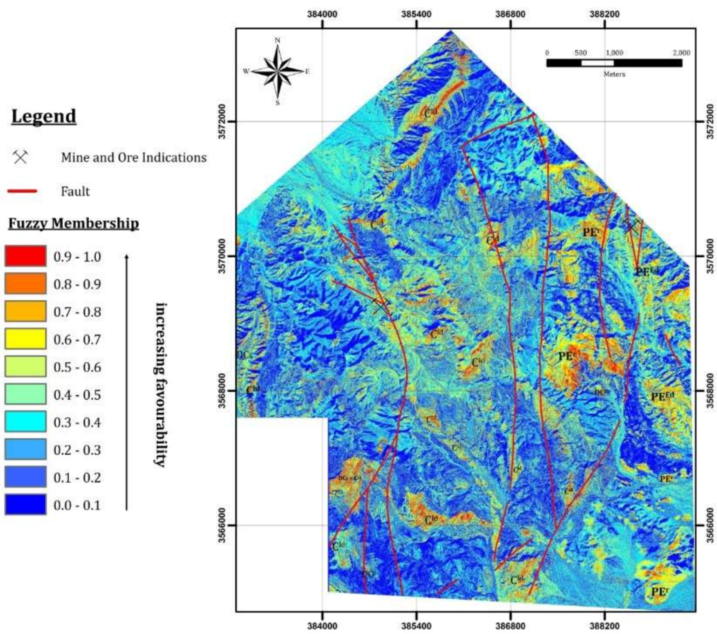

Figure 3. Mineral prospectivity map derived from WV-3 selected alteration thematic layers.

5. Conclusions

ASTER and WV-3 were processed to generate mineral prospectivity maps for the CIT area. The PC3, PC4, PC5 and PC8 of ASTER mapping the spatial distribution of Mg-Fe-OH/CO3 minerals, iron oxide/hydroxides, OH/S-O/CO3-bearing minerals and dolomitization were considered as thematic layers. The PC3, PC4 and PC6 images of WV-3 identifying iron-stained alteration, dolomite/Fe^{2+} and Fe^{3+}oxides were considered as thematic layers. The fuzzy-logic model was used to produce mineral prospectivity maps using alteration thematic layers, including the PC4, PC5 and PC8 of ASTER and the PC3, PC4 and PC6 thematic layers of WV-3. As a result, the most favorable/prospective zones for Pb-Zn mineralization in the study area were identified that can be considered for future exploration field campaign.

References

Abrams, M., Tsu, H., Hulley, G., Iwao, K., Pieri, D., Cudahy, T., Kargel, J., 2015. The Advanced Spaceborne Thermal Emission and Reflection Radiometer (ASTER) after fifteen years: Review of global products. International Journal of Applied Earth Observation and Geoinformation, 38, 292–301.

Clark, R.N., 1999. Spectroscopy of rock and minerals and principles of spectroscopy. In: Rencz, A.N. (Ed.) Remote Sensing for the Earth Sciences: Manual of Remote Sensing 3. John Wiley Sons, New York, pp. 3–58.

Govil, H., Gill, N., Rajendran, S., Santosh, M., Kumar, S., 2018. Identification of new base metal mineralization in Kumaon Himalaya, India, using hyperspectral remote sensing and hydrothermal alteration. Ore Geology Reviews, 92, 271-283.

Gupta R.P., Tiwari R.K., Saini, V., Srivastava, N. 2013. A simplified approach for interpreting principal component images. Advances in Remote Sensing 2, 111–119.

Hunt, G.R.; Ashley, R.P. 1979. Spectra of altered rocks in the visible and near-infrared. Econ. Geol. 74, 1613–1629.

Kim, Y. H., Choe, K. U., Ri, R. K. 2019. Application of fuzzy logic and geometric average: A Cu sulfide deposits potential mapping case study from Kapsan Basin, DPR Korea. Ore Geology Reviews, 107, 239-247.

Kuester, M., 2016. Radiometric use of WV-3 imagery. Technical Note. DigitalGlobe p. 12.

Mars, J.C., 2018. Mineral and Lithologic Mapping Capability of WorldView 3 Data at Mountain Pass, California, Using True- and False-Color Composite Images, Band Ratios, and Logical Operator Algorithms. Economic Geology, 113 (7), 1587–1601.

Mars, J. C. Rowan, L.C., 2011. ASTER spectral analysis and lithologic mapping of the Khanneshin carbonate volcano, Afghanistan. Geosphere, 7, 276-289.

Mars, J. C. Rowan, L.C., 2010. Spectral assessment of new ASTER SWIR surface reflectance data products for spectroscopic mapping of rocks and minerals. Remote Sens Environ 114: 2011–2025.

Novák, V.; Perfilieva, I.; Močkoř, J., 1999. Mathematical principles of fuzzy logic. Dordrecht: Kluwer Academic. ISBN 978-0-7923-8595-0.

Pour, A.B., Hashim, M., Hong, J.K., Park, Y., 2019a. Lithological and alteration mineral mapping in poorly exposed lithologies using Landsat-8 and ASTER satellite data: north-eastern Graham Land, Antarctic Peninsula. Ore Geology Reviews, 108, 112-133.

Pour, A.B., Park, Y., Crispini, L., Läufer, A., Kuk Hong, J., Park, T.-Y.S., Zoheir, B., Pradhan, B., Muslim, A.M., Hossain, M.S., Rahmani, O. 2019b. Mapping Listvenite Occurrences in the Damage Zones of Northern Victoria Land, Antarctica Using ASTER Satellite Remote Sensing Data. Remote Sensing 11, 1408. doi.org/10.3390/rs11121408

Pour, A.B., Park, T.-Y., Park, Y., Hong, J.K., Muslim, A.M., Läufer, A., Crispini, L., Pradhan, B., Zoheir, B., Rahmani, O., Hashim, M., Hossain, M.S., 2019c. Landsat-8, Advanced Spaceborne Thermal Emission and Reflection Radiometer, and WorldView-3 Multispectral Satellite Imagery for Prospecting Copper-Gold Mineralization in the Northeastern Inglefield Mobile Belt (IMB), Northwest Greenland. Remote Sens. 2019, 11, 2430. doi.org/10.3390/rs11202430.

Pour, A.B., Park, Y., Park, T.S., Hong, J.K. Hashim, M., Woo, J., Ayoobi, I. 2018a. Regional geology mapping using satellite-based remote sensing approach in Northern Victoria Land, Antarctica. Polar Science 16, 23-46.

Pour, A.B., Hashim, M., Park, Y., Hong, J.K. 2018b. Mapping alteration mineral zones and lithological units in Antarctic regions using spectral bands of ASTER remote sensing data. Geocarto International 33 (12), 1281-1306.

Pour, A.B., Park, T.S., Park, Y., Hong, J.K. Zoheir, B., Pradhan, B., Ayoobi, I. Hashim, M., 2018c. Application of multi-sensor satellite data for exploration of Zn-Pb sulfide mineralization in the Franklinian Basin, North Greenland. Remote Sensing 10, 1186; doi:10.3390/rs10081186.

Rajabi, A., Rastad, E., Canet, C., 2012. Metallogeny of Cretaceous carbonate-hosted Zn–Pb deposits of Iran: geotectonic setting and data integration for future mineral exploration. International Geology Review, 54(14), 1649–1672. doi:10.1080/00206814.2012.659110.

Samani, B. A., 1988. Metallogeny of the Precambrian in Iran. Precambrian research, 39(1-2), 85-106.

Zadeh, L.A. 1965. "Fuzzy sets". Information and Control 8 (3), 338–353. doi:10.1016/s0019-9958(65)90241